

# Laser-Microdissection of Protein Crystals Down to Submicron Dimensions

Eugenia Pechkova<sup>1,2</sup>, Luca Belmonte<sup>1</sup>, Christian Riekkel<sup>3</sup>, Dmitri Popov<sup>4</sup>, Christian Koenig<sup>5</sup> and Claudio Nicolini<sup>2\*</sup>

<sup>1</sup>Laboratories of Nanobiotechnology and Biophysics, University of Genova, 16132, Italy

<sup>2</sup>Corresponding author: Claudio Nicolini, Nanoworld Institute, Fondazione ELBA Nicolini, Pradalunga, Bergamo, 24020, Italy

<sup>3</sup>Experiments Division, European Synchrotron Radiation Facility, France

<sup>4</sup>HPCAT, Geophysical Laboratory, Carnegie Institution of Washington, USA

<sup>5</sup>Paul Scherrer Institute (PSI), Villigen, Switzerland

## Abstract

We studied laser-microdissection of standard and Langmuir-Blodgett (LB) nanotemplate protein crystals in glycerol solution. The time required for microdissection was significantly longer for LB-crystals as compared to standard-crystals which also more rapidly dissolve. Microfragmentation of lysozyme crystals was observed after extended solvent exposure. Synchrotron radiation nanobeam mapping allowed localizing and aligning cryofrozen lysozyme microfragments. 3D data-sets obtained from two microfragments were refined to atomic resolution. The well-defined electron density maps showed no evidence for damage of radiation of sensitive side-groups. Our results suggest applications of laser-microdissection techniques in structural studies on crystals with a high mosaicity. They also provide a new window for the characterization of protein crystal organization down to the submicron scale, pointing to a new emerging biophysical technique.

**Keywords:** Langmuir-Blodgett; Synchrotron radiation; X-ray topography; Lysozyme

## Introduction

While, a lot of efforts are being invested at Synchrotron Radiation (SR) sources on high-throughput protein-to-structure pipe-lines in the context of structural genomics [1-4], methods allowing manipulating and tailoring of protein micro-crystals in a laboratory or SR-beamline environment have been less explored. Such techniques could, however, be useful for separating and sorting crystals from a batch, for dissection of crystals, polymorphs or crystalline domains from an aggregate or a cellular environment. We also note the idealized model of a protein crystal composed of coherently scattering mosaic blocks [5] which can be experimentally studied by X-ray line-profile analysis or X-ray topography [6,7]. The properties and interactions of individual mosaic blocks are, however, rarely addressed. As an example we mention the observation of radiation damage induced accumulation of hydrogen at the mosaic-block boundaries of insulin crystals resulting in a reduction of block-size and increase of mosaicity [8,9]. A more detailed understanding of mosaic block interactions could contribute to more refined models of protein crystal mechanics and is of fundamental importance for defining the frontiers of nanomedicine [10,11]. Finally we note that raster-diffraction techniques allow identifying high-quality diffracting volume-elements in a batch of microcrystals or a larger crystal [12,13]. We are aware that the selection of mosaic blocks for X-ray nanodiffraction techniques would represent a methodological progress and could in particular improve the quality of structural refinements for high mosaicity crystals. For all of these reasons it is of interest exploring techniques allowing dissecting protein crystals, ultimately down to the level of individual mosaic blocks.

In view of the generally fragile nature of biological matter, laser-optical techniques appear to be well suited for protein crystal manipulation [9,14-16] and microdissection [17-25]. Our aim was exploring the ultimate size in coherently scattering crystal fragments obtainable by microdissection, principally for the model protein lysozyme. Preliminary results have been reported elsewhere in Pechkova and Nicolini [26]. In the following, we will use the term laser-microdissection for the cutting of a crystal by a laser beam while microfragmentation will be used for the separation of a microdissected

crystal into smaller fragments due to effects such as cavitations at domain boundaries and solvent interpenetration. Given the rather small microfragments obtained in the present study, we used X-ray nanocrystallography for localizing individual microfragments and collecting data sets. We were also interested in the question whether crystals differing in perfection and X-ray radiation stability differ also in microdissection and microfragmentation behavior. This issue is of importance for the generation of very small crystals which might be more prone to laser-radiation damage than larger crystals. We will compare in this paper the microdissection behavior of Langmuir-Blodgett (LB) based crystals (called LB-crystals) and crystals obtained by standard (e.g. hanging drop) crystallization techniques (called standard-crystals) for lysozyme. Indeed, LB-crystals appear to have significantly higher radiation stability as compared to standard crystals for a wide range of proteins [27-32]. The LB nanotemplate crystallization method was first introduced by Pechkova and Nicolini [26]. According to this method, based on LB nanotechnology [34], a LB protein monolayer deposited on the glass slide by means of Langmuir-Blodgett trough previously proved to be highly ordered and thermostable [34] in the common hanging-drop method causes the acceleration of the nucleation and the crystal growth rate [33,35,36]. During the last decade, LB nanotemplate crystallization method was successfully used for crystallization of the protein not crystallizable by classical crystallization techniques [31,37,38], for producing significantly more radiation stable [26,28-32] and higher quality crystals [31,32] in comparison with classical ones for a wide range of proteins. The reason of these LB crystals qualities is mostly due to the more compact inner water molecules organization

**\*Corresponding author:** Claudio Nicolini, Nanoworld Institute, Fondazione ELBA Nicolini, Pradalunga, Bergamo, 24029, Italy, Tel: +39-010-353-38217, E-mail: [cnicolini@ibf.unige.it](mailto:cnicolini@ibf.unige.it)

**Received** September 24, 2013; **Accepted** October 29, 2013; **Published** October 31, 2013

**Citation:** Pechkova E, Belmonte L, Riekkel C, Popov D, Koenig C, et al. (2013) Laser-Microdissection of Protein Crystals Down to Submicron Dimensions. J Nanomed Nanotechnol S15:002. doi:10.4172/2157-7439.S15-002

**Copyright:** © 2013 Pechkova E. This is an open-access article distributed under the terms of the Creative Commons Attribution License, which permits unrestricted use, distribution, and reproduction in any medium, provided the original author and source are credited.

in the structure [39]. In the present work, the higher stability of LB crystal allows successful X-ray nanodiffraction analysis of their microfragments after the laser microdissection.

## Methods

### Protein crystallization

Lysozyme protein crystals were obtained by a state-of-the-art crystallization technique based on Langmuir-Blodgett (LB) nanotemplates [28,40-47]. LB-nanofilms were generated by the LB-technique and its variation, a modified Langmuir-Schaeffer (LS) technique [27,28,42]. Typically, protein was spread at the air-water interface of an in-house LB-trough and immediately compressed with 70 cm/min to a surface pressure of ~20 mN/m. The protein monolayers were then transferred from the water surface onto siliconized cover slips by touching the support in parallel to the surface according to the LS-technique at a pressure of ~20 mN/m. These LB-nanofilms were then used as crystallization templates [28,31,39]. Lysozyme was crystallized from 40 mg/ml lysozyme in 50 mM sodium acetate solution using the hanging drop vapor diffusion method. Crystallization conditions were the same for standard- and LB-crystals. The 4  $\mu$ l droplet of protein solution was mixed with 4  $\mu$ l droplet of precipitant (0.9 M NaCl) on the glass cover slide covered with two LB lysozyme monolayers and equilibrated over reservoir containing 1ml of 0.9 M NaCl. Further details can be found in Pechkova and Nicolini [33].

### Laser-microdissection

Experiments were performed using a Zeiss PALM laser-microdissection system with a laser wavelength of  $\lambda=355$ nm and <2ns pulses of 90  $\mu$ J each at 100 Hz [48]. This corresponds for a ~4  $\mu$ m<sup>2</sup> laser spot to a laser fluency of ~562 J/cm<sup>2</sup> and a flux density of ~4\*10<sup>21</sup> photons s<sup>-1</sup> mm<sup>-2</sup>. The laser beam was focused on the surface of the crystal avoiding thus shockwave induced crack formation. In order to allow in-situ observation and manipulation of crystal cuts, we performed microdissection operations for all four proteins being utilized (standard and LB) initially in an open aqueous solution drop rather than in a flash-frozen cryoloop [22]. The freely floating protein crystals and the convective flow induced by evaporation did, however, not allow clear cuts. In addition, evaporation resulted also in salt precipitation which limited the time available for sample manipulation. The movement of crystals and fragments could, however, be significantly reduced by electrostatically fixing them to a mica sheet and using a more viscous (~20%) glycerol solution. This also reduced the evaporation rate and allowed subsequent cryocooling of the sample. The microdissected protein crystals were transferred from the drop into a cryoloop or cryomesh for flash-freezing [28,49]. This method could, however, not be used for the much smaller microfragments which were instead generated directly from protein crystals in glycerol solution, kept in a cryoloop. The cryoloop was transferred to a micromanipulator and aligned in the laser-beam for microdissection. In order to avoid evaporation of the thin glycerol film, we first froze the loop containing one or more lysozyme crystals, then cut a selected crystal at room temperature (r.t.) and finally froze the loop again. Crystals which were not hit by the laser beam did not show any degradation during this procedure. Two single shots resulted only in several larger fragments while longer waiting times resulted in a microfragmentation into crystallites down to about 1  $\mu$ m dimension (Figure 4). After microfragmentation the loops were flash-frozen to 100 K on the beamline microgoniometer.

### Synchrotron radiation experiments

We used the ID13 undulator beamline at the ESRF-Grenoble [50].

A monochromatic SR-beam of  $\lambda=0.09611$  wavelength was focused by crossed linear Fresnel lenses to a ~400 nm spot at the sample position [51]. The flux of ~7\*10<sup>10</sup> photons/s corresponded to a flux density of ~3\*10<sup>11</sup> ph/s/ $\mu$ m<sup>2</sup>. A scanning goniometer with integrated rotation axis was used to position and rotate the samples [52]. Samples were aligned normal to the beam by an on-axis Olympus microscope, which was calibrated to the beamline focal spot. Experiments were performed in transmission geometry at 100 K using an Oxford Cryoflow system. Diffraction data were collected by a MAR CCD 165 detector with 2K\*2K pixels of 78.94\*78.94  $\mu$ m<sup>2</sup> (binned to 1024\*1024 pixels) at a sample-to-detector distance of 114.41 mm (refined) for a typical exposure time/pattern of 1s and a 1° of rotation. Raster-diffraction experiments were performed in step-scanning mode along two orthogonal axes, normal to the SR-beam. The raster-diffraction experiments were analyzed with the FIT2D program [53].

### Data processing and refinement

The lysozyme data-sets were indexed and integrated with XDS [54,55], scaled with XDSCALE and converted with XDSCONV. Lysozyme spacegroup P4<sub>3</sub>2<sub>1</sub>2 was recognized by POINTLESS [56] and the data sets were processed in this spacegroup. Freerflag from the CCP4 [57] software package was used for the calculation of Free R factors ( $R_{\text{free}}$ ) [58]. According to the Matthews coefficient results [59,60], molecular replacement was performed with one molecule in the asymmetric unit assuming a protein mass of 14.3 KDa for lysozyme. Automated molecular replacement was performed using MOLREP using PDB templates with ID: 2AUB [61,62]. Both LB crystal fragments are solved by molecular replacement using the same template. 2AUB is the structure with the highest homology scoring of the Lysozyme LB structures. The PDB [63] file was then refined using REFMAC5 [64,65]. Before the final refinement step, electron density maps were inspected by COOT [66] at the same contour level. Dataset scaling was performed using both SCALA and Freerflag from the CCP4 software package [58]. In order to obtain significant statistics, data were processed at a resolution of 2.3 Å for the LB1 data set and 2.5 Å for the LB2 data set. The PDB file [63] was then refined for both datasets. Manipulation of PDB files was performed using RASMOL [67]. Visual inspection of protein structures was performed using PyMol [68].

## Results and Discussions

### Laser-microdissection

Microcrystals of lysozyme could be readily produced by laser-microdissection from LB-crystals while standard-crystals, obtained under the same conditions and of the same dimensions as LB crystals, disintegrated rapidly under the same conditions suggesting a lower stability. Indeed, cutting of lysozyme crystals along a user-defined line on the crystal required a continuous exposure of ~90 s to pulsing laser beam for LB-crystals and respectively ~20 s for standard-crystals. The cutting procedure is illustrated in Figures 1A and 1B. The crystal splits along the cutting surfaces immediately after being hit by a laser pulse. Within the first minutes after the onset of the cutting process, the characteristic fracture along lines could not be observed. Indeed, Figure 1A shows the crystal before cutting along the green line with the number 107 and Figure 1B after. The dissolution of a microdissected LB-crystal into microfragments after a waiting time is shown in Figures 1C and Figure 1D. The cutting of a standard-crystal into two parts is shown in Figures 2A and 2B. The surrounding solution developed a few larger black bubbles after a laser hit which did, however, not obstruct crystal observation. (Figure 2B) The cut surfaces of the two parts of the standard-crystal are not well defined and start breaking-up into smaller

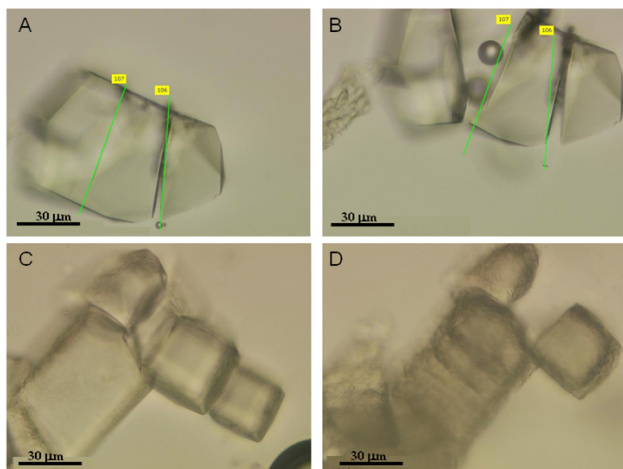


**Figure 1:** Lysozyme LB-crystal in 20% glycerol solution fixed to a mica substrate. The crystal has already been cut along the green line 106. A further cut along the green line 107 has been programmed; B: LB-crystal after the cut along line 107. The dissected crystal parts have started moving apart. Black bubbles are formed by the interaction of the laser beam with the liquid. C: Microdissected LB-crystals after 22 minutes; D: same crystals after 28 minutes.

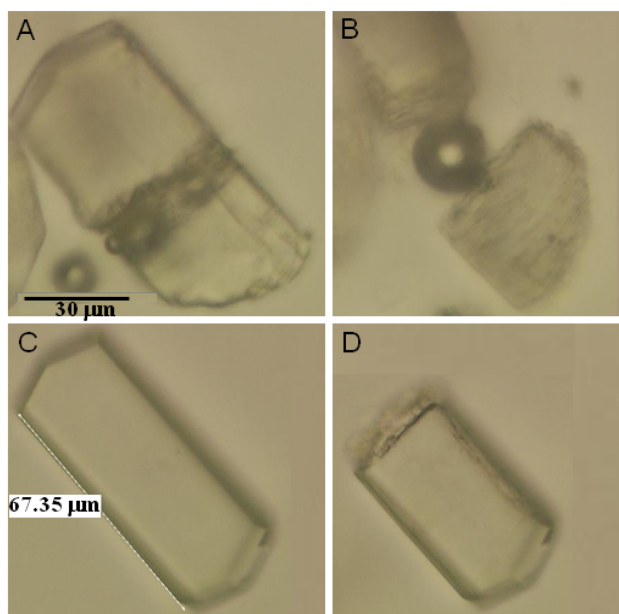


**Figure 2:** Laser-microdissection of lysozyme crystals in glycerol solution. A,B: Standard-crystals cut after exposure of ~20 sec to pulsing laser beam; The pictures show the same protein crystal during the cut (A) and shortly after the division of the two parts (B) with slightly rotated fragments; C: LB-crystals before microdissection; D: same crystal after ~90 sec laser beam exposure.

fragments (from 1 to 3  $\mu\text{m}$ ) during the cutting-process. In contrast, the LB-crystal splits into two parts with clean cutting surfaces without immediate formation of microfragments. (Figures 2C and Figure 2D) This implies that microfragmentation of standard-crystals proceeds at a higher rate than for LB-crystals. In larger crystals of  $\sim 50 \mu\text{m}$ , one single laser impulse can -when hit in the right place- induce the crystals to split along certain lines producing fragments with  $\sim 15 \mu\text{m}$  minimum size.

Microfragmentation into smaller anisotropic crystallites was observed for lysozyme after some time depending on the type of the crystal. (Figures 3A- Figure 3C) The crystal shapes started dissolving into rows of microfragments which took up to 30 minutes for a standard-crystal and more than 45 minutes for a LB-crystal. These differences were reproducible and suggest a higher stability of the LB-crystals. By hitting at lines between the microfragments it was easy separating them. (Figures 3A-Figure 3C) Indeed, Figure 3A shows a standard- crystal, 20 minutes after only two laser pulses focused on one point. The morphology revealed displays large differences between standard- and LB-crystals [26,43,44]. Images of microdissected and microfragmentated lysozyme LB-crystals in a cryoloop are shown in Figures 4A-4C. We tentatively attribute the microfragmentation of the cut crystals to a fast stress increase and cavitations at the domain boundaries induced by nanosecond laser flashes [69-71]. The shock waves have been shown to propagate hundreds of microns into biological matter such as cornea [70]. Slow interdiffusion of glycerol molecules is assumed to dissolve the hydrogen-bonded water network at the mosaic block boundaries resulting in their separation [72].

### Nanodiffraction of LB-crystal microfragments

The optical image quality of the cryofrozen lysozyme LB-microfragments was not sufficient to clearly observe them at the beamline. (Figure 4D) We performed therefore raster-diffraction with

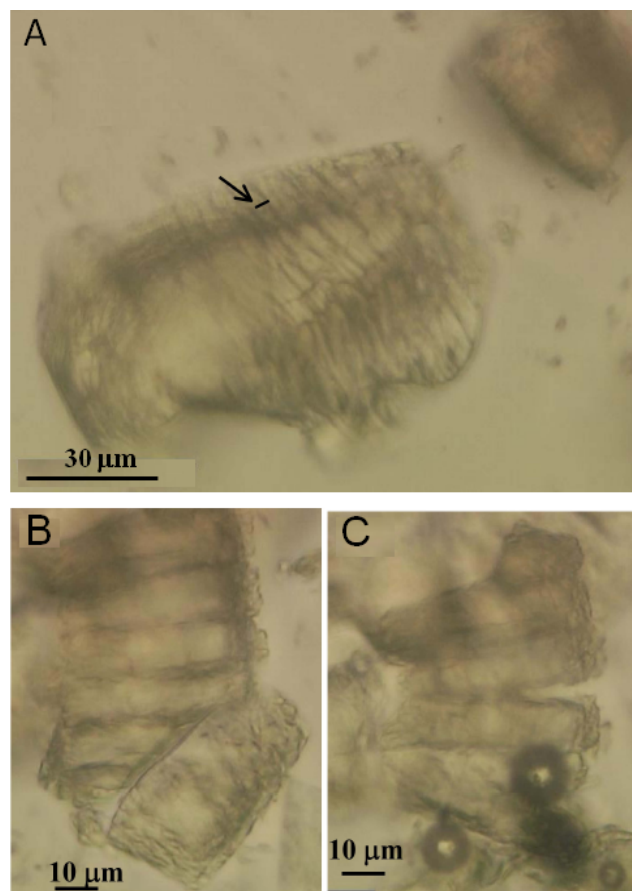
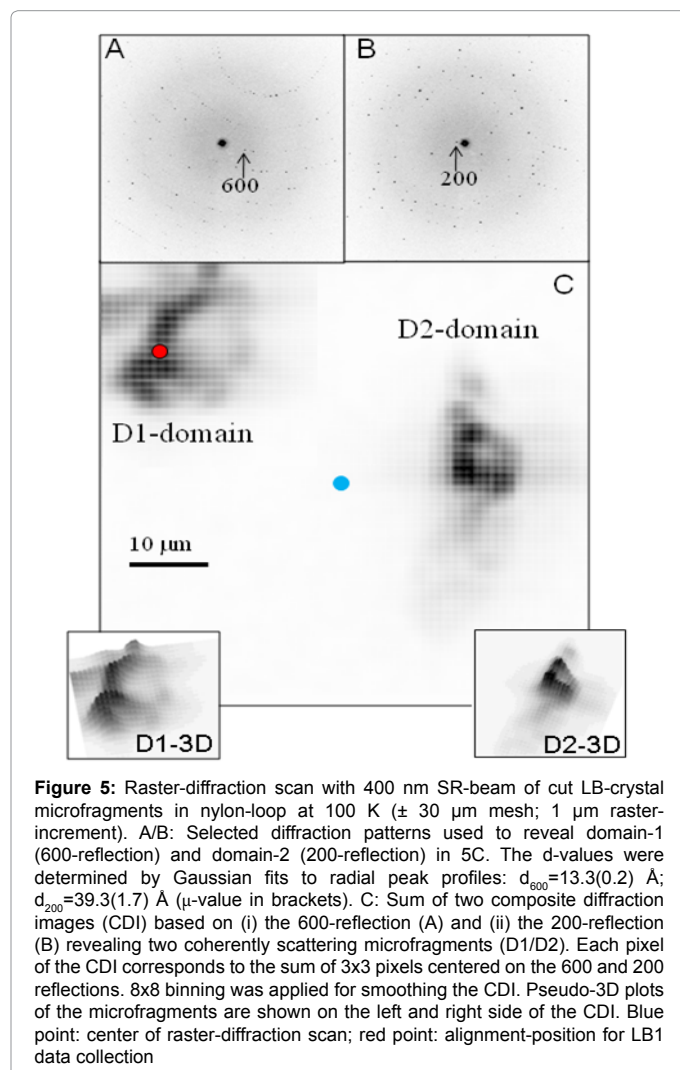
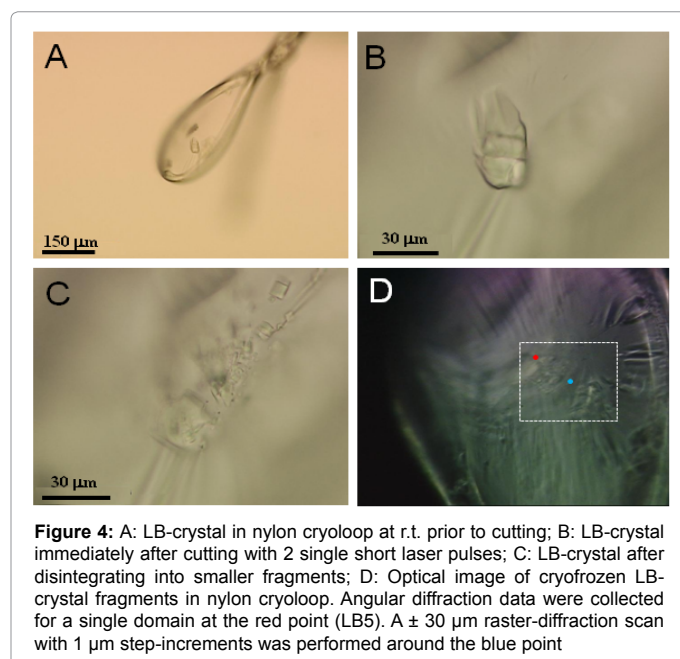


**Figure 3:** A: Standard-crystal in glycerol solution, 20 minutes after laser irradiation. The arrow indicates  $1 \mu\text{m}$  domains. B: Onset of microfragmentation in LB-crystal 40 min after laser irradiation; C: When hit with the laser, the microfragments easily split



an X-ray nanobeam to localize and align microfragments for single crystal data collection. A  $\pm 30 \mu\text{m}$  mesh-scan with  $1 \mu\text{m}$  step-increment revealed two zones in which the diffraction patterns indicated the presence of homogeneously diffracting volume elements (Figures 5A and 5B). We selected two low-order reflections (600/200) marked by arrows in Figure 5A, Figure 5B ( $d_{600}=13.3(0.2) \text{ \AA}$ ;  $d_{200}=39.3(1.7) \text{ \AA}$ ) to generate composite diffraction images (CDI) [73] revealing the two coherently scattering microfragments. (Figure 5C) The elongated projected scattering density of the two microfragments (called D1- and D2-domain) resembles roughly the size and shape of the microfragments shown in the optical images. (Figures 3B and 3C) We centered the D1-domain in the X-ray nanobeam (red point in Figures 4D and 6C) and collected a  $110^\circ$  data set with  $1^\circ$  angular increments. (LB1 data-set) The same procedure was performed for localizing a further homogeneously scattering domain in a 2<sup>nd</sup> cryofrozen sample (LB2 data-set). In this case we collected a  $180^\circ$  data set with  $1^\circ$  angular increments. We noticed that the illuminated volume for an estimated upper limit of microfragment thickness of  $5 \mu\text{m}$  is  $\leq 0.8 \mu\text{m}^3$  for a single exposure corresponding to  $\sim 3.5 \times 10^6$  unit cells. This relates to the lowest scattering power of reported protein structures based on SR microcrystallography [49,73].

High-resolution data-sets were collected by X-ray nanodiffraction for the LB1- and LB2-domains. (Figure 6) All diffraction images of the LB1 data-set contained processable diffraction spots. The 110 diffraction images from the LB2 data-set contained, however, only 50 images with processable diffraction spots, presumably due to crystal centering errors. Data refinement statistics for both data-sets showed excellent parameters such as low  $R_{\text{sym}}$ ,  $R_{\text{factor}}$  and  $R_{\text{free}}$ . (Table 1) The latter statistics is consistent with statistics for LB lysozyme crystal of standard dimensions [62], for instance, the structure with PDB access code 2AUB. Moreover statistics are quite similar to any Lysozyme crystal structure obtained by any classical hanging drop method in PDB or in our hands (4I8S). We also noted the low mosaicity values of  $\sim 0.3$  (LB1) and  $\sim 0.2$  (LB2) which are in the range expected for a beam divergence of  $\sim 1 \text{ mrad}$ . The 75% completeness for LB2 is reflected in a rather low redundancy of about 5.1. (Table 1) We find excellent electron densities for the LB1 and LB2 structures (Figure 7A) with practically identical structure overlaps of LB1 and LB2, made by superimposing processing via PyMol (not shown). The secondary structure of LB1 (and LB2) shows well-defined residues highlighted in the  $2F_o - F_c$  maps. (Figure 7A) Small differences are only observed for the  $\beta$ -sheets of both structures while other secondary structures seem to be identical. (Figures 7B and 7C) Electron density maps of both LB1 and LB2 reveal well-defined densities for all residues and do not show broken disulphide bridges for sensitive residues i.e. glutamates and decarboxylated aspartates. (Figures 7D and 7E) Similar results were obtained for a Xylanase II microcrystal and related to the photoelectron escape from the  $\sim 1 \mu\text{m}$  diameter diffraction channel [74]. This is also a reasonable assumption for the even smaller beam channel used in the present study. The enhanced radiation stability for LB-crystals might, however, also contribute to the observed radiation stability [30].

## Conclusions

Laser-microdissection of standard protein crystals poses problems as the cut surfaces of the two parts of the crystals are not well defined and start breaking-up into smaller fragments during the cutting-process. Clean cut surfaces can, however, be obtained for LB-crystals. Extended exposure of lysozyme LB-crystals to aqueous glycol solution allows separating the crystals into microfragments. The anisotropy of the microfragments appears to reflect anisotropic lysozyme mechanical properties [75]. Structural data from microfragments by

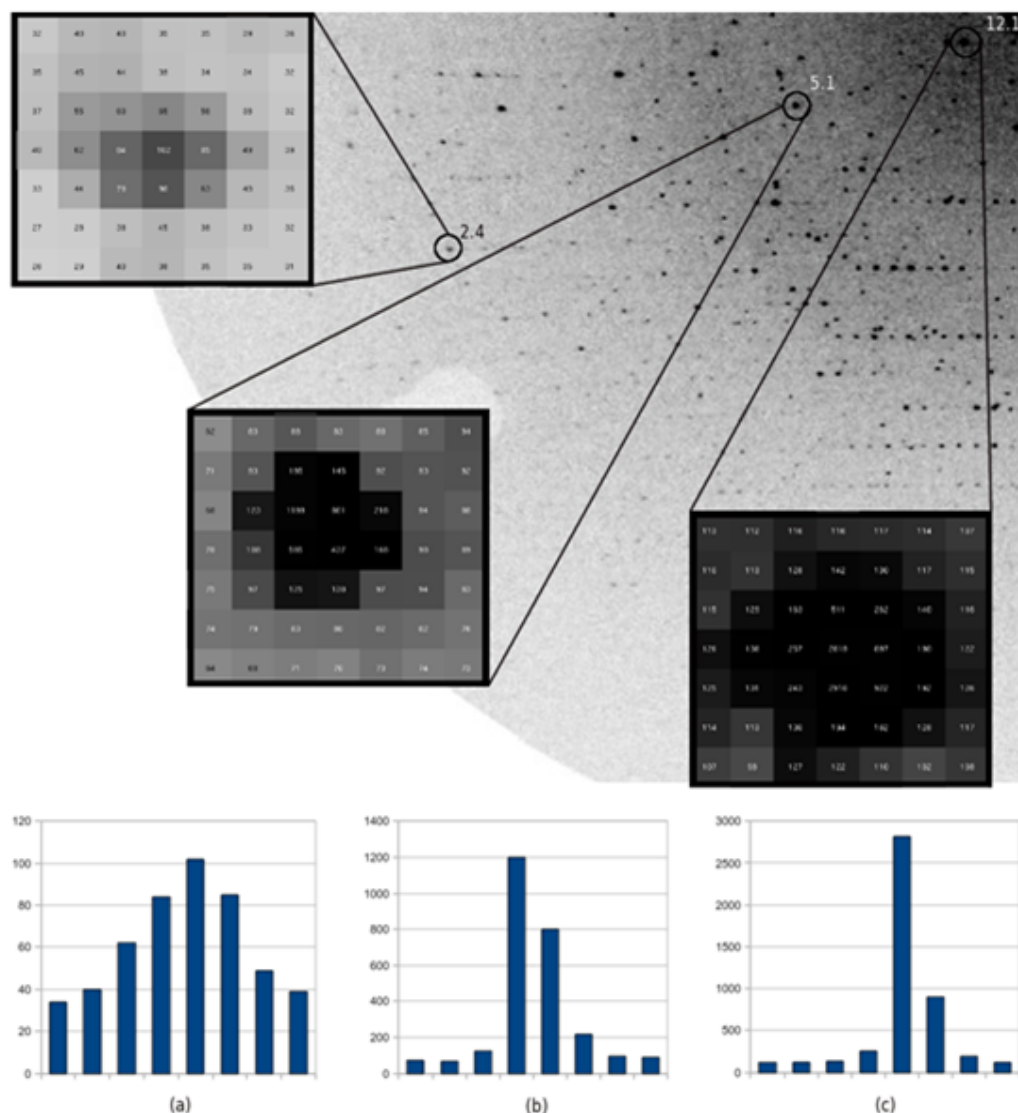


**Figure 6:** Diffraction pattern of lysozyme with spot shapes for reflections at different resolutions of about 2.4 Å (a), 5.1 Å (b) and 12.1 Å (c) shown as histograms, analogue to [74].

Parameters	4GG0	4GFZ
Resolution (Å)	2.3	2.5
Unit cell a,c (Å) (where a=b) $\alpha = \beta = \gamma = 90^\circ$	78.8, 37.1	79.7, 37.2
Spacegroup	P 4 <sub>3</sub> -2 <sub>1</sub> -2	P 4 <sub>3</sub> -2 <sub>1</sub> -2
Mosaicity (°)	~0.3	~0.2
R <sub>sym</sub>	0.21	0.16
R-factor	0.19	0.20
R <sub>free</sub>	0.28	0.32
I/ $\sigma$ (values in brackets correspond to the outer resolution shell Å)	13.5 (6.9)	9.1 (4.9)
Redundancy	13.6	5.1
Completeness (%)	100	75.23
Total number of reflections	5284	3205
Mean B-value for side chains	14.8	10.7
R.m.s. on bond length (Å)	0.015	0.014
R.m.s. in bond angle (Å)	1.5	1.5
N° of water molecules	78	47

**Table 1:** Lysozyme LB-crystal structural parameters obtained by nanodiffraction for 4GG0 (LB1) and 4GFZ (LB2).

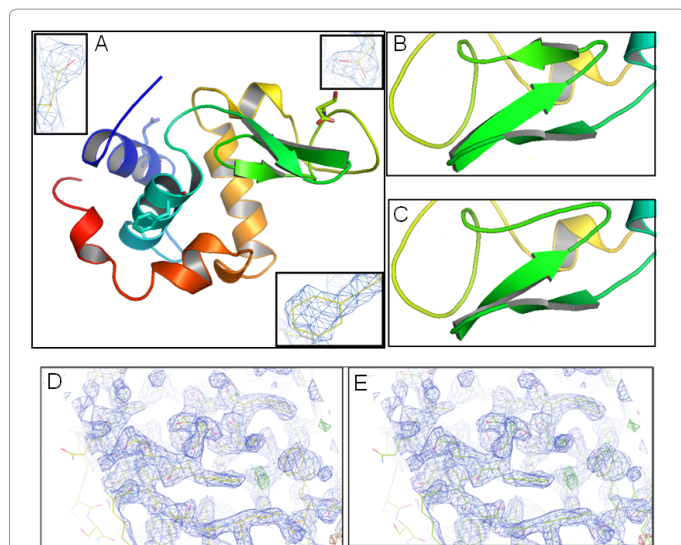


**Figure 7:** A: LB1 lysozyme structure. Selected residues are highlighted with a 1.69 Å resolution ( $\sigma$ ) in the 2Fo-Fc map on a contour level of  $0.78e \text{ \AA}^{-3}$ . Residues are 14 (ARG), 66 (ASP) and 34 (PHE) from the left up corner clockwise. B: Details of differences in secondary structure for LB1; C: same for LB2. D: Electron density map for LB1; E: same for LB2.

nanocrystallography correspond to a quality obtained by standard protein crystallography. Electron density maps reveal that radiation damage effects do not play a key role in agreement with other studies. The combination of LB technology for protein crystallography with laser cutting and nanobeam data acquisition opens therefore new crystallographic possibilities in particular for crystals which are notorious for their high mosaicity such as membrane protein crystals. We also noticed that microfragmentation of protein crystals in a microfluidic environment could provide a source of nanocrystals for serial crystallography experiments at ultrahigh brilliance X-ray sources [76].

Laser-microdissection method was here proved able to obtain pieces of crystals with dimensions so small to be considered quite-domain. This method can be used before X-ray micro and nanodiffraction techniques in order to overcome the very common problem of twinned, defect, aggregated and mosaic crystals. Indeed, the mosaicity in microdissected fragments was reduced in respect to standard structures. Therefore, we envision that this method could be useful also for the crystals with high mosaicity such membrane protein crystals, which can be object of future studies in this field. While the very small microcrystals fragments of several domain size are often believed not suitable for the complete data collection by conventional X-ray crystallography, in the case of LB nanotemplate crystallization highly radiation resistant combined with X-ray nanodiffraction and Laser microdissection this is here proved possible.

Despite this approach requires rather sophisticated nanotechnologies to be applied, in addition to the robust lysozyme several other model proteins (thaumatin, ribonuclease and insulin) were successfully studied at the micron scale with the same procedure using Laser and LB and with similar results [77].

## Supporting Material

The atomic coordinates and structural factors have been deposited in the Protein Data Bank ([www.pdb.org](http://www.pdb.org)). LB1: PDB ID code 4GG0,

RCSB ID code is RCSB074134; LB2: PDB ID code 4GFZ, RCSB ID code is RCSB074135.

## Acknowledgement

We thank Dr. I Snigireva of the ESRF microimaging laboratory for help with the use of the PALM MicroBeam microdissection system. We thank Dr. M. Burghammer for instrumental support at the ID13 beamline. This work was supported by FIRB-MIUR grants to Claudio Nicolini of the University of Genoa for Functional Proteomics (RBNE01X3CE) and for Nanosensors (RBPR05JH2P) and by a MIUR grant to the Fondazione E.I.B.A. for Funzionamento (DM48527).

## References

1. Brockhauser S, Svensson O, Bowler MW, Nanao M, Gordon E, et al. (2012) The use of workflows in the design and implementation of complex experiments in macromolecular crystallography. *Acta Crystallogr D Biol Crystallogr* 68: 975-984.
2. Eisliger MA, Deacon AM, Godzik A, Lesley SA, Wooley J, et al. (2010) The JCSG high-throughput structural biology pipeline. *Acta Crystallogr Sect F Struct Biol Cryst Commun* 66: 1137-1142.
3. Liu ZJ, Tempel W, Ng JD, Lin D, Shah AK, et al. (2005) The high-throughput protein-to-structure pipeline at SECSG. *Acta Crystallogr D Biol Crystallogr* 61: 679-684.
4. Beteva A, Cipriani F, Cusack S, Delageniere S, Gabadinho J, et al. (2006) High-throughput sample handling and data collection at synchrotrons: embedding the ESRF into the high-throughput gene-to-structure pipeline. *Acta Crystallogr D Biol Crystallogr* 62: 1162-1169.
5. Nave C (1999) Matching X-ray source, optics and detectors to protein crystallography requirements. *Acta Cryst D* 55: 1663-1668.
6. Lübbert D, Meents A, Weckert E (2004) Accurate rocking-curve measurements on protein crystals grown in a homogeneous magnetic field of 2.4 T. *Acta Crystallogr D Biol Crystallogr* 60: 987-998.
7. Helliwell JR (2005) Protein crystal perfection and its application. *Acta Crystallogr D Biol Crystallogr* 61: 793-798.
8. Meents A, Gutmann S, Wagner A, Schulze-Briese C (2010) Origin and temperature dependence of radiation damage in biological samples at cryogenic temperatures. *Proc Natl Acad Sci U S A* 107: 1094-1099.
9. Santucci SC, Cojoc D, Amenitsch H, Marmiroli B, Sartori B, et al. (2011) Optical tweezers for synchrotron radiation probing of trapped biological and soft matter objects in aqueous environments. *Anal Chem* 83: 4863-4870.
10. Buehler M J (2006) Mechanics of protein crystals: Atomistic modeling of elasticity and fracture. *Journal of Theoretical and Computational Nanotechnology* 3: 670-683.
11. Nicolini C, Pechkova E (2010) Nanoproteomics for nanomedicine. *Nanomedicine (Lond)* 5: 677-682.
12. Cherezov V, Hanson MA, Griffith MT, Hilgart MC, Sanishvili R, et al. (2009) Rastering strategy for screening and centring of microcrystal samples of human membrane proteins with a sub-10 microm size X-ray synchrotron beam. *J R Soc Interface* 6: S587-S597.
13. Bowler MW, Guisjarro M, Petitdemange S, Baker I, Svensson O, et al. (2010) Diffraction cartography: applying microbeams to macromolecular crystallography sample evaluation and data collection. *Acta Crystallogr D Biol Crystallogr* 66: 855-864.
14. Hikima T, Shimizu T, Yamamoto M (2008) Manipulating orotein microcrystals with optical tweezers based on lensed fiber probes. *Acta Cryst A* 64: C313-314.
15. Wagner A, Metcalf P, Ward A (2008/2009) Protein microcrystal manipulation with optical tweezers. Rutherford Appleton Laboratory, Laser For Science Facility (LSF).
16. Santucci SC, Amenitsch H, Cojoc D, Riekkel C (2012) Synchrotron Radiation and Structural Proteomics. Pechkova E, Riekkel C (Ed.), Pan Stanford Publishing, Singapore 183-212.
17. Kashii M, Hosokawa Y, Kitano H, Adachi H, Mori Y, et al. (2007) Femtosecond laser-induced cleaving of protein crystal in water solution. *Appl Surf Sci* 253: 6447-6450.
18. Kashii M, Kitano H, Hosokawa Y, Adachi H, Mori Y, et al. (2005) Femtosecond Laser Processing of Protein Crystals in Crystallization Drop. *Japanese Journal of Applied Physics Part 2-Letters* 43: L873-L875.

19. Kitano H, Adachi H, Murakami A, Matsumura H, Takano K, et al. (2004) Protein crystal processing using a deep-UV laser. *Japanese Journal of Applied Physics Part 2-Letters* 43: L73-L75.
20. Kitano H, Adachi H, Murakami A, Matsumura H, Takano K, et al. (2004) New approach to improve X-ray diffraction pattern of protein crystal using UV-laser ablative processing. *Japanese Journal of Applied Physics Part 2-Letters* 43: L297-L299.
21. Kitano H, Adachi H, Sato A, Murakami A, Matsumura H, et al. (2004) Application of UV-Laser Ablation to Detaching Protein Crystal from Growth Vessel. *Japanese Journal of Applied Physics Part 2-Letters* 43: L1271-L1274.
22. Kitano H, Matsumura H, Adachi H, Murakami S, Takano K, et al. (2005) Protein cryocrystallography using laser-processed crystal. *Jpn J Appl Phys* 44: L54-L56.
23. Kitano H, Murakami S, Adachi H, Matsumura H, Takano K, et al. (2005) Processing of membrane protein crystal using ultraviolet laser irradiation. *J Biosci Bioeng* 100: 50-53.
24. Kitano H, Sato A, Murakami A, Adachi H, Matsumura H, et al. (2004) Novel approach to process protein crystals using deep-UV laser Fifth International Symposium on Laser Precision Microfabrication 5662: 280-284.
25. Murakami A, Kitano H, Adachi H, Matsumura H, Takano K, et al. (2004) Universal processing technique for protein crystals using pulsed UV laser. *Japanese Journal of Applied Physics Part 2-Letters* 43: L873-L876.
26. Pechkova E, Nicolini C (2010) Domain organization and properties of LB lysozyme crystals down to submicron size. *Anticancer Res* 30: 2745-2748.
27. Nicolini C, Pechkova E (2006) Nanostructured biofilms and biocrystals. *J Nanosci Nanotechnol* 6: 2209-2236.
28. Pechkova E, Nicolini C (2004) Protein nanocrystallography: a new approach to structural proteomics. *Trends Biotechnol* 22: 117-122.
29. Pechkova E, Tripathi S, Ravelli RB, McSweeney S, Nicolini C (2009) Radiation stability of proteinase K crystals grown by LB nanotemplate method. *J Struct Biol* 168: 409-418.
30. Belmonte L, Pechkova E, Tripathi S, Scudieri D, Nicolini C (2012) Langmuir-Blodgett nanotemplate and radiation resistance in protein crystals: state of the art. *Crit Rev Eukaryot Gene Expr* 22: 219-232.
31. Pechkova E, Zanotti G, Nicolini C (2003) Three-dimensional atomic structure of a catalytic subunit mutant of human protein kinase CK2. *Acta Crystallogr D Biol Crystallogr* 59: 2133-2139.
32. Pechkova E, Scudieri D, Belmonte L, Nicolini C (2012) Oxygen-bound Hell's gate globin I by classical versus LB nanotemplate method. *J Cell Biochem* 113: 2543-2548.
33. Pechkova E, Nicolini C (2001) Accelerated protein crystal growth by protein thin film template. *J Cryst Growth* 231: 599-602.
34. Pechkova E, Sivozhelezov V, Nicolini C (2007) Protein thermal stability: the role of protein structure and aqueous environment. *Arch Biochem Biophys* 466: 40-48.
35. Pechkova E, Nicolini C (2002) Protein nucleation and crystallization by homologous protein thin film template. *J Cell Biochem* 85: 243-251.
36. Pechkova E, Nicolini C (2002) From art to science in protein crystallization by means of thin-film nanotechnology. *Nanotechnology* 13: 460-464.
37. Pechkova E, Tripathi S, Spera R, Nicolini C (2008) Groel crystal growth and characterization. *Biosystems* 94: 223-227.
38. Pechkova E, Vasile F, Spera R, Nicolini C (2008) Crystallization of alpha and beta subunits of IF2 translation initiation factor from archaeobacteria *Sulfolobus solfataricus*. *Journal of Crystal Growth*, 310: 3767-3770.
39. Pechkova E, Sivozhelezov V, Belmonte L, Nicolini C (2012) Unique water distribution of Langmuir-Blodgett versus classical crystals. *J Struct Biol* 180: 57-64.
40. Pechkova E, Vasile F, Spera R, Fiordoro S, Nicolini C (2005) Protein nanocrystallography: growth mechanism and atomic structure of crystals induced by nanotemplates. *J Synchrotron Radiat* 12: 772-778.
41. Pechkova E, Fiordoro S, Fontani D, Nicolini C (2005) Investigating crystal-growth mechanisms with and without LB template: protein transfer from LB to crystal. *Acta Crystallogr D Biol Crystallogr* 61: 809-812.
42. Nicolini C (1997) Protein-monolayer engineering: principles and application to biocatalysis. *Trends in Biotechnology* 15: 395-401.
43. Nicolini C, Pechkova E (2010) An overview of nanotechnology-based functional proteomics for cancer and cell cycle progression. *Anticancer Res* 30: 2073-2080.
44. Pechkova E, Sartore M, Giacomelli L, Nicolini C (2007) Atomic force microscopy of protein films and crystals. *Rev Sci Instrum* 78: 093704.
45. Pechkova E, Nicolini C (2004) Atomic structure of a CK2alpha human kinase by microfocus diffraction of extra-small microcrystals grown with nanobiofilm template. *J Cell Biochem* 91: 1010-1020.
46. Pechkova E, Tropiano G, Riekkel C, Nicolini C (2004) Radiation stability of protein crystals grown by nanostructured templates: synchrotron microfocus analysis *Spectrochimica Acta B59*: 1687-1693.
47. Pechkova E, Innocenzi P, Malfatti L, Kidchob T, Gaspa L, et al. (2007) Thermal stability of lysozyme Langmuir-Schaefer films by FTIR spectroscopy. *Langmuir* 23: 1147-1151.
48. [www.zeiss.de/microdissection](http://www.zeiss.de/microdissection) (2012)
49. Riekkel C, Burghammer M, Popov D (2012) Synchrotron Radiation and Structural Proteomics. Pechkova E, Riekkel C (Ed), Pan Stanford Publishing, Singapore.
50. Riekkel C, Burghammer M, Davies R, Gebhardt R, Popov D (2009) Applications of Synchrotron Light to Scattering and Diffraction in Materials. Ezquerra TA, Garcia-Gutierrez M, Nogales A, Gomez M (Ed.), Springer, Heidelberg, Germany.
51. Noehammer B, David C, Burghammer M, Riekkel C (2005) Coherence-matched microfocusing of hard X-rays. *Appl Phys Lett* 86: 16310-16314.
52. Volkringer C, Popov D, Loiseau T, Guillou N, Ferey G, et al. (2007) A microdiffraction set-up for nanoporous metal-organic-framework-type solids. *Nat Mater* 6: 760-764.
53. Hammersley A (2009) The FIT2D Home Page.
54. Kabsch W (2010) XDS. *Acta Crystallogr D Biol Crystallogr* 66: 125-132.
55. Kabsch W (2010) Integration, scaling, space-group assignment and post-refinement. *Acta Crystallogr D Biol Crystallogr* 66: 133-144.
56. Evans P (2006) Scaling and assessment of data quality. *Acta Crystallogr D Biol Crystallogr* 62: 72-82.
57. Collaborative Computational Project, Number 4 (1994) The CCP4 suite: programs for protein crystallography. *Acta Crystallogr D Biol Crystallogr* 50: 760-763.
58. Brünger AT (1997) Free R value: cross-validation in crystallography. *Methods Enzymol* 277: 366-396.
59. Kantardjiev KA, Rupp B (2003) Matthews coefficient probabilities: Improved estimates for unit cell contents of proteins, DNA, and protein-nucleic acid complex crystals. *Protein Sci* 12: 1865-1871.
60. Matthews BW (1968) Solvent content of protein crystals. *J Mol Biol* 33: 491-497.
61. Vagin A, Teplyakov A (1997) MOLREP: an Automated Program for Molecular Replacement. *Journal of Applied Crystallography* 30: 1022-1025.
62. Pechkova E, Sivozhelezov V, Tropiano G, Fiordoro S, Nicolini C (2005) Comparison of lysozyme structures derived from thin-film-based and classical crystals. *Acta Crystallogr D Biol Crystallogr* 61: 803-808.
63. Berman H, Henrick K, Nakamura H (2003) Announcing the worldwide Protein Data Bank. *Nat Struct Biol* 10: 980.
64. Murshudov GN, Vagin AA, Dodson EJ (1997) Refinement of macromolecular structures by the maximum-likelihood method. *Acta Crystallogr D Biol Crystallogr* 53: 240-255.
65. Murshudov G N, Vagin AA, Lebedev A, Wilson K S, Dodson E J (1999) Efficient anisotropic refinement of macromolecular structures using FFT. *Acta Cryst D* 55: 247-255.
66. Emsley P, Lohkamp B, Scott WG, Cowtan K (2010) Features and development of Coot. *Acta Crystallogr D Biol Crystallogr* 66: 486-501.
67. Sayle RA, Milner-White EJ (1995) RASMOL: biomolecular graphics for all. *Trends Biochem Sci* 20: 374.

- 
68. PyMol (2012) The PyMOL Molecular Graphics System, Schrödinger, LLC. Version 1.5.0.4.
69. Hosokawa Y, Yashiro M, Asahi T, Masuhara H M (2001) *Laser Applications in Microelectronic and Optoelectronic Manufacturing VI*, p. 78. San Jose, CA, USA.
70. Juhasz T, Hu X H, Turi L, Bor Z (1994) Dynamics of shock waves and cavitation bubbles generated by picosecond laser pulses in corneal tissue and water. *Laser Surg Med* 15: 91-98.
71. Tang W, Weidner DA, Hu BY, Newton RJ, Hu XH (2006) Efficient delivery of small interfering RNA to plant cells by a nanosecond pulsed laser-induced stress wave for posttranscriptional gene silencing. *Plant Sci* 171: 375-381.
72. Dashnau JL, Nucci NV, Sharp KA, Vanderkooi JM (2006) Hydrogen bonding and the cryoprotective properties of glycerol/water mixtures. *J Phys Chem B* 110: 13670-13677.
73. Riekkel C, Burghammer M, Schertler G (2005) Protein crystallography microdiffraction. *Curr Opin Struct Biol* 15: 556-562.
74. Moukhametzianov R, Burghammer M, Edwards PC, Petitdemange S, Popov D, et al. (2008) Protein crystallography with a micrometre-sized synchrotron-radiation beam. *Acta Crystallogr D Biol Crystallogr* 64: 158-166.
75. Zamiri A, De S (2010) Modeling the mechanical response of tetragonal lysozyme crystals. *Langmuir* 26: 4251-4257.
76. Chapman HN, Fromme P, Barty A, White TA, Kirian RA, et al. (2011) Femtosecond X-ray protein nanocrystallography. *Nature* 470: 73-77.
77. Nicolini C, Belmonte L, Riekkel C, Popov D, Koenig C, Pechkova E (2013) *Am J Biochem Biotechnol*.